REPORT DOCUMENTATION PAGE

Public reporting burden for this collection of information is estimated to average 1 hour per response, including the time for reviewing instructions, searching existing data sources, gathering and maintaining the data needed, and completing and reviewing this collection of information. Send comments regarding this burden estimate or any other aspect of this collection of information, including suggestions for reducing this burden to Department of Defense, Washington Headquarters Services, Directorate for Information Operations and Reports (0704-0188), 1215 Jefferson Davis Highway, Suite 1204, Arlington, VA 22202-4302. Respondents should be aware that notwithstanding any other provision of law, no person shall be subject to any penalty for failing to comply with a collection of information if it does not display a currently valid OMB control number. **PLEASE DO NOT RETURN YOUR FORM TO THE ABOVE ADDRESS.**

1. REPORT DATE (DD-MM-YYYY)	2. REPORT TYPE		3. DATES COVERED (From - To)
15-12-2001	Journal Article		2001

4. TITLE AND SUBTITLE	5a. CONTRACT NUMBER
Thermal hysteresis loop, dynamical breakdown, and emission-current spike in quantum-well photodetectors	
	5b. GRANT NUMBER
	5c. PROGRAM ELEMENT NUMBER
	62601F

6. AUTHOR(S)	5d. PROJECT NUMBER
Danhong Huang, Christian Morath, D.A. Cardimona, and Anjali Singh	4846
	5e. TASK NUMBER
	CR
	5f. WORK UNIT NUMBER
	C1

7. PERFORMING ORGANIZATION NAME(S) AND ADDRESS(ES)	8. PERFORMING ORGANIZATION REPORT NUMBER
Air Force Research Laboratory Space Vehicles Directorate 3550 Aberdeen Ave., SE Kirtland AFB, NM 87117-5776	

9. SPONSORING / MONITORING AGENCY NAME(S) AND ADDRESS(ES)	10. SPONSOR/MONITOR'S ACRONYM(S)
	11. SPONSOR/MONITOR'S REPORT NUMBER(S)

12. DISTRIBUTION / AVAILABILITY STATEMENT
Approved for Public Release; Distribution is Unlimited.

13. SUPPLEMENTARY NOTES

14. ABSTRACT
A nonabiabatic sequential-tunneling model is developed and applied to explore the common origin of the transient behavior of electrons in quantum-well photodetectors in the presence of different time-dependent external sources, including device temperature, electric field, and incident optical flux. For the time-dependent temperature, a counterclockwise hysteresis loop in the tunneling current as a function of the swept temperature is predicted and attributed to a blockade or an enhancement of the sequential tunneling of electrons between quantum wells by the space-charge-field effect when the device temperature is swept up and then down. When a time-dependent electric field is applied, a dynamical breakdown of the photodetectors is predicted, where the peak of total current linearly increases with the frequency of an ac electric field from its static value under a dc field. This is due to the presence of an additional dielectric current, which is proportional to the oscillation frequency of the ac electric field and whose peak value becomes larger than the value of the saturated tunneling-current peak in the high-frequency domain. Under the dynamical-breakdown condition, the quantum-well photodetectors behave just like a uniform dielectric medium. In the presence of a time-dependent optical flux, an emission-current spike is predicted as a result of the dominant enhancement of the escape probability of electrons from quantum wells over the loss of electron density when an applied dc electric field is small. The experimental observations of the transient behavior of electrons in quantum-well photodetectors are successfully reproduced by our numerical calculations.

15. SUBJECT TERMS
photodectors, multiple quantum wells, nonadiabatic, hystersis

16. SECURITY CLASSIFICATION OF:			17. LIMITATION OF ABSTRACT	18. NUMBER OF PAGES	19a. NAME OF RESPONSIBLE PERSON
a. REPORT	**b. ABSTRACT**	**c. THIS PAGE**	Unlimited	13	Mr. David Cardimona
Unclassified	Unclassified	Unclassified			**19b. TELEPHONE NUMBER** (include area code) (505) 846-5807

Thermal hysteresis loop, dynamical breakdown, and emission-current spike in quantum-well photodetectors

Danhong Huang,[a] Christian Morath, D. A. Cardimona, and Anjali Singh[b]
Air Force Research Lab (AFRL/VSSS), 3550 Aberdeen Avenue S. E., Building 426, Kirtland Air Force Base, New Mexico 87117

A nonadiabatic sequential-tunneling model is developed and applied to explore the common origin of the transient behavior of electrons in quantum-well photodetectors in the presence of different time-dependent external sources, including device temperature, electric field, and incident optical flux. For the time-dependent temperature, a counterclockwise hysteresis loop in the tunneling current as a function of the swept temperature is predicted and attributed to a blockade or an enhancement of the sequential tunneling of electrons between quantum wells by the space-charge-field effect when the device temperature is swept up and then down. When a time-dependent electric field is applied, a dynamical breakdown of the photodetectors is predicted, where the peak of total current linearly increases with the frequency of an ac electric field from its static value under a dc field. This is due to the presence of an additional dielectric current, which is proportional to the oscillation frequency of the ac electric field and whose peak value becomes larger than the value of the saturated tunneling-current peak in the high-frequency domain. Under the dynamical-breakdown condition, the quantum-well photodetectors behave just like a uniform dielectric medium. In the presence of a time-dependent optical flux, an emission-current spike is predicted as a result of the dominant enhancement of the escape probability of electrons from quantum wells over the loss of electron density when an applied dc electric field is small. The experimental observations of the transient behavior of electrons in quantum-well photodetectors are successfully reproduced by our numerical calculations. [DOI: 10.1063/1.1415760]

I. INTRODUCTION

In a recent article, Singh and Cardimona reported a discovery of a residual dark current in quantum-well photodetectors (QWIPs) when an ac bias voltage sweeps through zero. Later, Hubbs *et al.*[2] observed a rolloff of the dynamical responsivity in QWIPs when the frequency of a chopped incident optical flux is increased beyond a certain value. More recently, Choi *et al.*[3] experimentally found a counterclockwise hysteresis loop for the tunneling current and a clockwise hysteresis loop for the emission current in QWIPs as the device temperature was swept up from 10 to 300 K and then back down.

A phenomenological circuit model[1] was proposed that successfully explained the observed zero-bias residual dark current in numerical simulations. After that, a quantum-mechanical model[4] was developed to explore the microscopic origin of the residual dark current. This led to the discovery of the current instability and hysteresis loop in QWIPs. For the rolloff of the responsivity in QWIPs as a function of the chopper frequency, Huang *et al.*[5] have put forward a quantum theory that numerically reproduced and physically explained this experimental phenomenon. A scheme based on the nonadiabatic model[4,5] was proposed to

eliminate this responsivity rolloff using a small ac bias to compensate the charge-density fluctuations in quantum wells (QWs) that occur with a changing incoming optical flux.

Here, we raise the following question: Is there a common microscopic origin for all these experimental phenomena, including the zero-bias residual dark current, the rolloff of the dynamical responsivity, and the thermal hysteresis loops for both the tunneling and emission currents in QWIPs? We have found the answer to this question to be yes, the charge-density fluctuations in QWs induced by a nonadiabatic sequential-tunneling or photoemission process. It is well known that resonant electron tunneling in QWIPs can occur only when the barrier between adjacent wells is thin. If the barrier is very thick, the phase of the wave function will be completely lost as an electron tunnels from one well to the next. As a result, only sequential tunneling of electrons exists for thick barriers. If the QWIPs are only subject to constant external sources, such as device temperature, bias voltage, and incident optical flux, electrons in the QWs remain in a steady state with a fixed electron density. However, when the external sources become time dependent, electrons in QWs can no longer remain in this steady state. Instead, electrons will migrate through a series of intermediate transient states. The chemical potential of electrons in any one of these states suffers a fluctuation from the time-dependent external sources, and electron sequential tunneling between adjacent wells changes from an adiabatic process to

[a]Author to whom correspondence should be addressed: electronic mail: danhong.huang@kirtland.af.mil
[b]Also at JDS Uniphase Corporation, Monmonth Executive Center, 100 Willowbrook Road, Building 1, Freehold, NJ 07728-2879.

a nonadiabatic one. As a result, the charge density of electrons in the QWs starts to fluctuate around the value of the doping density, which either blocks or promotes the tunneling of electrons via a nonadiabatic space-charge-field effect when the QWs are charged or discharged, respectively.

In this article, we propose a nonadiabatic sequential-tunneling model containing a chemical-potential fluctuation for QWIPs in the presence a time-dependent external source. On the basis of this model, we derive a dynamical equation with respect to a nonadiabatic electric field describing the charge-density fluctuations in QWs. Using the derived dynamical equation subject to a time-dependent device temperature, we successfully reproduce and explain the observed hysteresis loop[3] for the tunneling current as a function of device temperature in QWIPs. A completely different physical mechanism behind this thermal hysteresis loop will be provided compared to the interpretation given by Choi *et al.*[3] We also report on the dynamical breakdown of QWIPs observed in our experiment and we elucidate the physics of this phenomenon. In addition, an explanation of the previously observed emission-current spike by Hubbs *et al.*[2] when an optical shutter is opened will be provided.

The organization of this article is as follows. In Sec. II, we present our nonadiabatic sequential-tunneling model and theory to study the transient behavior of QWIPs in the presence of a time-dependent device temperature, electric field, and incident optical flux. The thermal hysteresis loop, dynamical breakdown, and emission-current spike observed experimentally in QWIPs are successfully reproduced and the common origin of all these transient behaviors is explored. Numerical results and discussions are given in Sec. III, for three different cases, including an ac electric field, a chopped optical flux, and a time-dependent device temperature. Some previous and current experimental data from other groups and our experiments are also displayed in this section for a qualitative comparison. The article is concluded in Sec. IV with some remarks.

II. MODEL AND THEORY

In this section, we start by considering a typical QWIP sample which consists of GaAs layers for the QWs and $Al_xGa_{1-x}As$ layers for the barriers separating adjacent wells. The thickness (width) of the barriers (wells) is $L_B(L_W)$, and the depth of the wells is U_0. The effective mass of electrons is m^*. An electric field is applied to the sample in the z (growth) direction. The donors are uniformly distributed within each QW and assumed to be ionized to give rise to an electron density n_{2D} in a QW.

The sequential-tunneling electrons in a QWIP will remain in a steady state when a constant electric field or a constant optical flux has been applied to the system at any fixed temperature. In this case, a steady-state current will flow between the emitter and collector of the system, and the charge density in each QW will be kept at a constant n_{2D} (the applied electric field is assumed to be uniform inside the QWIP). However, a small current surge which is superposed on this steady-state current will be created[4,5] in the system whenever the chemical potential μ_c of electrons in the sys-

tem undergoes a fluctuation $\Delta\mu_c$ due to an external time-dependent source such as device temperature $T_e(t)$ or electric field $\mathcal{E}_b(t)$. The current surge is so small that its effect cannot be seen in a resonant-tunneling process within a superlattice. However, in a sequential-tunneling process the current surge can induce up to 20% charge-density fluctuations in the QWs,[5] which leads to a measurable nonadiabatic tunneling current. By using Levine's sequential-tunneling model[6] for electrons, the tunneling-current surge can be quantitatively described by[4]

$$I_t^s(t) = eSv_d(\mathcal{E}_b)\left(\frac{m^*}{\pi\hbar^2 L_W}\right)\int_0^{+\infty} dE\, \mathcal{T}(E,\mathcal{E}_b)$$

$$\times\left\{f_0\left[\frac{E+E_1-\mu_c-\Delta\mu_c}{k_B T_e}\right] - f_0\left[\frac{E+E_1-\mu_c}{k_B T_e}\right]\right\}, \quad (1)$$

where $f_0(x) = (1+e^x)^{-1}$ is the Fermi–Dirac distribution function, S is the area for the cross section of the sample, $v_d(\mathcal{E}_b)$ is the drift velocity of electrons[4] under an electric field $\mathcal{E}_b$, E_1 is the ground-state energy of electrons in each QW, and $\mathcal{T}(E,\mathcal{E}_b)$ is the instantaneous transmission coefficient of electrons through a biased barrier between adjacent wells.[7] During the sequential-tunneling process, an electron sees an instantaneous value of the electric field due to an extremely fast tunneling process (in the range of 1 ps) compared to the time (in the range of 1 ms–1 s) required for the appreciable change in $\mathcal{E}_b(t)$. In order to see an explicit time dependence of $\mathcal{T}(E,\mathcal{E}_b)$, a microwave field with the oscillation frequency exceeding 1–10 MHz must be employed, where a time-dependent Schrödinger equation must be solved to include the time dependence in the transmission coefficient through a dynamical barrier.[8]

Equation (1) of our model is based on the following facts. First, there exists a fluctuation $\Delta\mu_c$ in the chemical potential of the electron gas in each QW whenever either the bias field or the temperature varies with time. Second, $\Delta\mu_c$ will further introduce a conduction-current surge I_t^s. As a result, it causes a charge-density fluctuation in each quantum well, which in turn induces a time-dependent space-charge field. Finally, the generation of the dynamical space-charge field should be determined by the current-charge conservation law. This model has been successfully applied to explain the zero-bias offset of the tunneling current[4] and the frequency rolloff of the responsivity[5] observed experimentally. For fixed electron density in each QW, μ_c is a function of the electron temperature. If the temperature suffers from a fluctuation, it induces $\Delta\mu_c$. Similarly, if a bias field suffers from a fluctuation, some electrons will be accelerated while others will be decelerated. The imbalance of the electron energy disturbs the electron distribution and causes $\Delta\mu_c$. If the period of a time-dependent electric field is much larger than the tunneling time but smaller than the charging/discharging time of electrons in QWs, the electron motion is nonadiabatic in nature. The origin of the nonadiabatic motion of electrons is I_t^s represented by Eq. (1).

We would further like to point out that in the Levine's description[6] of the quantum sequential-tunneling current of electrons the two-dimensional tunneling current is effectively treated as a three-dimensional tunneling density (3DTD)[4]

moving with a drift velocity under a bias voltage through a thick barrier layer between two QWs in QWIPs, as can be seen from Eq. (1). The electrons contributing to 3DTD have energies expanded from the edge of the ground subband up to infinity, which includes the contributions of both thermionic and tunneling currents, although the density-of-states in Levine's formula[6] can be replaced by a 3D one when the electron energy is above the barrier. The effect of the energy barrier to electrons is included as a tunneling transmission coefficient in 3DTD, while the spatial scattering of electrons by imperfections in an alloy barrier layer is included in the drift velocity. Therefore, the drift velocity is appropriate for not only the electrons above the barriers but also the electron within the barriers.

Photoexcited emission current exists in QWIPs as a response to an incident optical flux. The generation of an emission current is probably a process involving photon-assisted electron tunneling as indicated by Levine.[6] It consists of two successive processes. The first step is the optical absorption by electrons, which lifts the electrons from a lower ground state to an upper excited state in the QWs. The second step involves the tunneling of photoexcited electrons out of the QWs through a biased barrier to a continuum state. This mechanism for producing an emission current, which is due to nonadiabatic photoexcitation, is obviously quite different from that for producing the tunneling currents described previously. Emission current is excited-state transport, while tunneling current is transport in the ground state. The detailed form of $I_e^s(t)$ will be given in Sec. II C.

The existence of either $I_t^s(t)$ or $I_e^s(t)$ will cause a deviation of the tunneling current in the system away from its steady-state value and, consequently, fluctuations of the charge density of electrons in each QW.[4,5] Here, the electrons no longer remain in the initial steady state with a time-independent tunneling current but instead move through a series of intermediate transient states with charge-density fluctuations and a dynamical tunneling current. However, the induced charge-density fluctuations in the QWs will be compensated by the concomitant change of the time-dependent tunneling current compared to its initial steady-state value and the system will eventually reach a final steady state with a different static tunneling current after a characteristic time (in the range of 1 s) similar to the charging/discharging time of a capacitive system in classical electrodynamics.[1]

A. Time-dependent device temperature $T_e(t)$

When the electron temperature $T_e(t)$ is varied with time t, the chemical potential $\mu_c(T_e)$ (for simplicity, the dependence of μ_c on the fixed electric field is not shown) of electrons in each QW is shaken up by a fluctuation $\Delta\mu_c = \tau_r[\partial\mu_c/\partial T_e][dT_e(t)/dt]$, where $\tau_r \sim 0.1-1$ ps is a parameter reflecting the energy-relaxation time of electrons back to an equilibrium state through intrasubband scattering.[9] If a parabolic energy dispersion is adopted for the electron motion within the quantum-well plane (perpendicular to the growth direction), we find the chemical potential of electrons for fixed n_{2D} to be

$$\mu_c(T_e) = E_1 + k_B T_e \ln\left[\exp\left(\frac{\pi\hbar^2 n_{2D}}{m^* k_B T_e}\right) - 1\right]. \qquad (2)$$

From Eq. (2) we find $\partial\mu_c/\partial T_e < 0$. By using Eq. (1), the dynamics of the charge-density fluctuation, described by $\mathcal{E}_{na}(t)$ in each QW is found to be determined by[4,5]

$$C_{QW}[\mathcal{E}_{na}(t)]\frac{d\mathcal{E}_{na}(t)}{dt} = \left[\frac{eS m^* v_d(\mathcal{E}_b)\tau_r}{\pi\hbar^2 k_B T_e(t) L_W L_B}\right]\frac{\partial\mu_c}{\partial T_e}\frac{dT_e(t)}{dt}$$

$$\times \int_0^{+\infty} dE \mathcal{T}(E,\mathcal{E}_b) f_0\left[\frac{E + E_1 - \mu_c(T_e)}{k_B T_e(t)}\right]$$

$$\times \left\{1 - f_0\left[\frac{E + E_1 - \mu_c(T_e)}{k_B T_e(t)}\right]\right\} - \left(\frac{1}{L_B}\right)$$

$$\times \{I_t[\mathcal{E}_b + \mathcal{E}_{na}(t), T_e(t)] - I_t[\mathcal{E}_b, T_e(t)]\}, \qquad (3)$$

where the dynamical quantum-well capacitance is

$$C_{QW}[\mathcal{E}_{na}(t)] = f_0\left[\frac{E_1 + eL_B\mathcal{E}_{na}(t) - \mu_c(T_e)}{k_B T_e}\right]\left(\frac{m^* e^2 S}{\pi\hbar^2}\right). \qquad (4)$$

In Eq. (3), $\mathcal{E}_{na}(t)$ is a nonadiabatic electric field which is associated with the charge-density fluctuation in each QW,[4] and $I_t[\mathcal{E}_b, T_e(t)]$ can be calculated using Levine's sequential-tunneling model.[4–6]

The capture process of carriers flowing above the barriers[10] has not been neglected in Eq. (4) although it has not been explicitly shown. For the tunneling process [including either a time-dependent temperature $T_e(t)$ here or a time-dependent electric field $\mathcal{E}_b(t)$ in Sec. II B], the difference between the capture and tunnel-emission currents is $I_t[\mathcal{E}_b(t) + \mathcal{E}_{na}(t), T_e(t)] - I_t[\mathcal{E}_b(t), T_e(t)]$. Here, we would like to emphasize that the difference between the capture and emission currents originates from the nonadiabatic current surge in our model. For the tunneling process, the current surge results from $\Delta\mu_c$ [$\propto dT_e(t)/dt$ here or $d\mathcal{E}_b(t)/dt$ in Sec. II B] in each QW. The nonadiabatic current surge survives even under a *uniform* time-dependent electric field and it reflects the quantum property of electrons in the QWs. This quantum effect is absent in the previous theories under a *nonuniform* electric field,[11,12] where the change of charge density with time in QWs results from the redistribution of a nonuniform bias field at each time.

The simplest example of a time-dependent device temperature to help visualize the physics involved in Eq. (3) is the step function: $T_e(t) = T_1 + (T_2 - T_1)\theta(t - t_1)$ which steps at $t = t_1$. From Eq. (3) we know that electrons with chemical potential $\mu_c(T_1)$ are knocked away by $I_t^s(t)$ at $t = t_1$ from their initial steady state due to $dT_e(t_1)/dt \neq 0$. As a result, the charge density in each QW fluctuates as $t > t_1$ due to the tunneling-current surge. If $dT_e(t_1)/dt > 0$ ($T_2 > T_1$), we find $\mathcal{E}_{na}(t) < 0$ for $t > t_1$, which means electrons will be sucked in and leads to the QWs being charged. During this time, the electrons are no longer in the initial steady state with a time-independent tunneling current but instead have moved through a series of intermediate transient states. The buildup of electrons in the QWs, however, decreases the tunneling current $I_t[\mathcal{E}_b + \mathcal{E}_{na}(t), T_2] < I_t[\mathcal{E}_b, T_2]$ with time for $t > t_1$.

This will bring in less electrons to each QW and eventually stabilize the electrons to a final steady state with a higher tunneling current $I_t[\mathcal{E}_b, T_2]$ and different chemical potential $\mu_c(T_2)$ but the same electron density n_{2D}. The facts that $I_t[\mathcal{E}_b + \mathcal{E}_{na}(t), T_2] < I_t[\mathcal{E}_b, T_2]$ with $T_1 < T_2$ and $I_t[\mathcal{E}_b + \mathcal{E}_{na}(t), T_2] > I_t[\mathcal{E}_b, T_2]$ with $T_1 > T_2$ during a series of intermediate transient states give rise to a counterclockwise *thermal hysteresis loop*[3] in $I_t[\mathcal{E}_b + \mathcal{E}_{na}(t), T_e(t)]$ versus $T_e(t)$ when the electron temperature $T_e(t)$ is swept up and then down with time. In this case, the tunneling current at a certain temperature $T_e(t)$ depends on the history of the variation of $T_e(t)$, namely, $dT_e(t)/dt$.

B. Time-dependent electric field $\mathcal{E}_b(t)$

If the applied electric field $\mathcal{E}_b(t)$ is time dependent, the chemical potential $\mu_c(\mathcal{E}_b)$ (for simplicity, the dependence of μ_c on the fixed electron temperature is not shown) of electrons in each QW again fluctuates with $\Delta\mu_c = \tau_t[\partial\mu_c/\partial\mathcal{E}_b][d\mathcal{E}_b(t)/dt]$, where $\tau_t \sim 0.01-1$ μs is a parameter associated with the electron sequential-tunneling time, which can be evaluated using the ratio of electron charge to the tunneling current.[13] For a parabolic-dispersion model, we find from Eq. (2) that $\partial\mu_c/\partial\mathcal{E}_b = dE_1(\mathcal{E}_b)/d\mathcal{E}_b$ for fixed T_e and n_{2D}, which relates to the Stark shift[14] of the ground-state energy of electrons in the QWs. With the help of Eq. (1), the dynamics of the charge-density fluctuation in the QWs can be obtained from[4,5]

$$C_{QW}[\mathcal{E}_{na}(t)]\frac{d\mathcal{E}_{na}(t)}{dt} = \left[\frac{eSm^*v_d[\mathcal{E}_b(t)]\tau_t}{\pi\hbar^2 k_B T_e L_W L_B}\right]\frac{\partial\mu_c}{\partial\mathcal{E}_b}\frac{d\mathcal{E}_b(t)}{dt}$$

$$\times \int_0^{+\infty} dE\, T[E, \mathcal{E}_b(t)] f_0\left[\frac{E + E_1(0) - \mu_c(0)}{k_B T_e}\right]$$

$$\times \left\{1 - f_0\left[\frac{E + E_1(0) - \mu_c(0)}{k_B T_e}\right]\right\} - \left(\frac{1}{L_B}\right)$$

$$\times \{I_t[\mathcal{E}_b(t) + \mathcal{E}_{na}(t), T_e] - I_t[\mathcal{E}_b(t), T_e]\}, \qquad (5)$$

where $E_1(0)$ and $\mu_c(0)$ are the ground-state energy and chemical potential of electrons in QWs at $\mathcal{E}_b = 0$ and $I_t[\mathcal{E}_b(t), T_e]$ can be calculated using Levine's sequential-tunneling model.[4–6] If we formally introduce an effective quantum-well capacitance according to

$$C_{eff} = \left[\frac{v_d[\mathcal{E}_b(t)]\tau_t}{L_B L_W}\right]\frac{dE_1(\mathcal{E}_b)}{d\mathcal{E}_b}\left\{\frac{m^*eS}{\pi\hbar^2 k_B T_e}\right\}$$

$$\times \int_0^{+\infty} dE\, T[E, \mathcal{E}_b(t)] f_0\left[\frac{E + E_1(0) - \mu_c(0)}{k_B T_e}\right]$$

$$\times \left\{1 - f_0\left[\frac{E + E_1(0) - \mu_c(0)}{k_B T_e}\right]\right\} \qquad (6)$$

and notice that $\tau_t T[E, \mathcal{E}_b(t)] \sim L_B/v_d[\mathcal{E}_b(t)]$ and $dE_1(\mathcal{E}_b)/d\mathcal{E}_b \sim eL_W$, we get $C_{eff} \sim C_{QW}[0]$ as can be obtained from Eq. (4) by setting $\mathcal{E}_{na}(t) = 0$. Under this condition, Eq. (5) will reduce to the previous dynamical equation.[4] We can easily understand the physics implied by Eq. (5) again using a step function $\mathcal{E}_b(t) = \mathcal{E}_1 + (\mathcal{E}_2 - \mathcal{E}_1)\theta(t - t_1)$ which steps at time $t = t_1$. For $t < t_1$, the electrons remain in an initial steady state with a relative chemical potential

$\mu_c(\mathcal{E}_1) - E_1(\mathcal{E}_1) = \mu_c(0) - E_1(0)$ (independent of $\mathcal{E}_b(t)$ although the electron wave functions depend on it[4]) in each QW. Because $d\mathcal{E}_b(t_1)/dt \neq 0$, the electrons in the QWs are pushed away from their initial steady state. This leads to charge density fluctuations in each QW for $t > t_1$. If $d\mathcal{E}_b(t_1)/dt > 0(\mathcal{E}_2 > \mathcal{E}_1)$ is assumed, we find $\mathcal{E}_{na}(t) > 0$ for $t > t_1$, indicating a discharging status for the QWs. However, this will increase the tunneling current $I_t[\mathcal{E}_2 + \mathcal{E}_{na}(t), T_e] > I_t[\mathcal{E}_2, T_e]$ with time for $t > t_1$, which pours more electrons into the discharged QWs to compensate for the charge loss and helps the electrons establish a final steady state with a higher tunneling current $I_t[\mathcal{E}_2, T_e]$ but the same relative chemical potential $\mu_c(\mathcal{E}_2) - E_1(\mathcal{E}_2) = \mu_c(0) - E_1(0)$ and electron density n_{2D}. From Eq. (5) we know that the tunneling current $I_t[\mathcal{E}_b(t) + \mathcal{E}_{na}(t), T_e]$ in the system depends on the nonadiabatic electric field $\mathcal{E}_{na}(t)$ and the oscillation frequency Ω_b of $\mathcal{E}_b(t)$ through $d\mathcal{E}_b(t)/dt$. Our numerical studies have discovered that the peak of $I_t[\mathcal{E}_b(t) + \mathcal{E}_{na}(t), T_e]$ as a function of Ω_b saturates to a maximum value $\sim I_t[(1 + C_{eff}/C_{QW}[0])\mathcal{E}_0, T_e]$ when Ω_b is very large, where $\mathcal{E}_0$ is the amplitude of a sinusoidal $\mathcal{E}_b(t)$. Within the saturation regime, the peaks of the tunneling current and $\mathcal{E}_b(t)$ are in-phase with each other completely, and the maximum value of the tunneling current changes with T_e and $\mathcal{E}_0$. On the other hand, we know from classical electrodynamics[15] that there exists a dielectric current $\epsilon_0\epsilon_r S d\mathcal{E}_b(t)/dt$ flowing through a QWIP if the well and barrier layers between the emitter and collector are viewed as a uniform dielectric medium (in addition to the QWs doped with electrons) with ϵ_r being their average dielectric constant. This dielectric current which does not contribute to change density in QWs increases linearly with Ω_b and becomes negligible when Ω_b is small. It has a $\pi/2$ phase shift with respect to $\mathcal{E}_b(t)$. Once the peak of the dielectric current becomes larger than the maximum value of the tunneling current as Ω_b is large enough, QWIPs suffer from a *dynamical breakdown*, i.e., the QWIP will just behave like a uniform dielectric medium. In this case, the current flowing inside a QWIP is dominated by the dielectric current instead of the conduction current.

C. Time-dependent optical flux $\Phi_{ph}(t)$

In the presence of a time-independent electric field $\mathcal{E}_b$ and incident optical flux, the electrons in both tunneling and emission channels of a QWIP remain in their steady state. In this case, the matching of the emission and capture currents keeps the electron density in each well at a constant n_{2D}.[6] However, if we apply a time-dependent optical flux $\Phi_{ph}(t)$ to the system, a mismatch between the active emission and passive capture currents occurs[5] due to a current surge, leading to charge-density fluctuations. As mentioned at the beginning of this section, the mechanism for producing the emission current is quite different from that for producing the tunneling current. Instead of using Eq. (1), the emission-current surge due to the nonadiabatic photoexcitation process is found to be[5]

$$I_e^s(t) = -\left(\frac{I_e[\mathcal{E}_b, \Phi_{ph}(t)]\tau_i}{\Phi_{ph}(t)}\right)\frac{d\Phi_{ph}(t)}{dt}, \qquad (7)$$

where $I_e[\mathcal{E}_b,\Phi_{ph}(t)]$ is the steady-state emission current, which can be calculated by using Levine's photoemission model,[6] and $\tau_i \sim 0.1-1$ ps is related to the lifetime of electrons in the upper excited state.[6] $I_e^s(t)$ will induce both a charge-density fluctuation in each QW and a deviation of the emission and tunneling currents from their steady-state values $I_e[\mathcal{E}_b,\Phi_{ph}(t)]$ and $I_t[\mathcal{E}_b,T_e]$. By using Eq. (7), the dynamical equation describing the charge-density fluctuation in each QW with dual conducting channels is found to be[5]

$$
\begin{aligned}
C_{QW}[\mathcal{E}_{na}(t)]\frac{d\mathcal{E}_{na}(t)}{dt} \\
= \left(\frac{\tau_i}{L_B\Phi_{ph}(t)}\right)I_e[\mathcal{E}_b,\Phi_{ph}(t)]\frac{d\Phi_{ph}(t)}{dt} - \left(\frac{1}{L_B}\right) \\
\times \{I_e[\mathcal{E}_b,\Phi_{ph}(t)] - I_t[\mathcal{E}_b,T_e] \\
- I_e[\mathcal{E}_b+\mathcal{E}_{na}(t),\Phi_{ph}(t)] + I_t[\mathcal{E}_b+\mathcal{E}_{na}(t),T_e]\}.
\end{aligned}
\tag{8}
$$

Here, the nonadiabatic emission current with $\mathcal{E}_{na}(t) \neq 0$ is calculated by[6]

$$
\begin{aligned}
I_e[\mathcal{E}_b+\mathcal{E}_{na}(t),\Phi_{ph}(t)] \\
= \left(\frac{m^*eS}{\pi\hbar^2}\right)\Phi_{ph}(t)P_e[\mathcal{E}_b+\mathcal{E}_{na}(t)]\sigma_{op}[\omega_{ph},\mathcal{E}_b+\mathcal{E}_{na}(t)] \\
\times \int_0^{+\infty} dE f_0\left[\frac{E+E_1(0)+eL_B\mathcal{E}_{na}(t)-\mu_c(0)}{k_BT_e}\right],
\end{aligned}
\tag{9}
$$

and $I_t[\mathcal{E}_b,T_e]$ is still given by Levine's sequential-tunneling model,[4–6] where $E_1(0)$ and $\mu_c(0)$ (for simplicity, the dependence of μ_c on the fixed electron temperature is not shown) still represent the ground-state energy and chemical potential of electrons in the QWs at $\mathcal{E}_b=0$, $\hbar\omega_{ph}$ is the incident photon energy, $P_e[\mathcal{E}_b]$ and $\sigma_{op}[\omega_{ph},\mathcal{E}_b]$ are the escape probability and optical cross section of electrons.[5]

In Eq. (9), the capture process of carriers flowing above the barriers has been implicitly included. In fact, for the photoemission process with a time-dependent optical flux $\Phi_{ph}(t)$, the difference between the capture and emission currents becomes $I_t[\mathcal{E}_b+\mathcal{E}_{na}(t),T_e] - I_t[\mathcal{E}_b,T_e] + I_e[\mathcal{E}_b,\Phi_{ph}(t)] - I_e[\mathcal{E}_b+\mathcal{E}_{na}(t),\Phi_{ph}(t)]$. Moreover, the capture probability p_c has been explicitly included in the previous calculation for the reponsivity $\mathcal{R}_{sp}$.[5] Here, we would like to indicate that the difference between the capture and emission currents in our model comes from the nonadiabatic excitation of electrons [$\propto d\Phi_{ph}(t)/dt$] from the ground state to the first excited state in the QW.

If we choose a step function $\Phi_{ph}(t)=\Phi_1+(\Phi_2-\Phi_1)\theta(t-t_1)$ stepping at time $t=t_1$, we know from Eq. (8) that the electrons will migrate away from the initial steady state because of $d\Phi_{ph}(t_1)/dt \neq 0$. Consequently, the electron charge density fluctuates in each QW as $t>t_1$. If $d\Phi_{ph}(t_1)/dt>0$ ($\Phi_2>\Phi_1$) is taken as an example, we find $\mathcal{E}_{na}(t)>0$ for $t>t_1$. This implies that the QWs are being discharged during this time. The increasing tunneling current $I_t[\mathcal{E}_b+\mathcal{E}_{na}(t),T_e]>I_t[\mathcal{E}_b,T_e]$ with time for $t>t_1$ adds more electrons to each QW to compensate for the charge loss. Eventually, the electrons in the QWs transit to a final steady state with a higher emission current $I_e[\mathcal{E}_b,\Phi_2]$ but the same

TABLE I. GaAs/Al$_{0.3}$Ga$_{0.7}$As QWIP sample 1 used in our numerical calculation with saturation velocity v_s, saturation field $\mathcal{E}_s$, cross-sectional area S, electron density n_{2D}, and relative dielectric constant ϵ_r.

v_s (10^6 cm/s)	$\mathcal{E}_s$ (kV/cm)	S (10^{-4} cm^{-2})	n_{2D} (10^{11} cm^{-2})	ϵ_r
2	2	2.25	4.1	11.2

chemical potential and electron density due to the establishment of a match between the emission and capture currents in the steady state. The nonadiabatic emission current $I_e[\mathcal{E}_b+\mathcal{E}_{na}(t),\Phi_2]$ can be either larger or smaller than the steady-state value of the emission current $I_e[\mathcal{E}_b,\Phi_2]$, depending on the competition between the loss of electron density in the QWs, seen as the term containing $\mu_c(0)-eL_B\mathcal{E}_{na}(t)-E_1(0)$ in Eq. (9), and the enhancement of the escape probability $P_e[\mathcal{E}_b+\mathcal{E}_{na}(t)]$ due to the additional lowering of the barrier by the nonadiabatic electric field. We note that the increase of the nonadiabatic electric field $\mathcal{E}_{na}(t)$ due to $d\Phi_{ph}(t_1)/dt>0$ makes the enhancement of the escape probability dominant through its exponential dependence on it[6] under certain conditions. However, the loss of charge density in each QW, which tends to reduce the final-state emission current $I_e[\mathcal{E}_b+\mathcal{E}_{na}(t),\Phi_2]$, will eventually dominate at a later time due to $0 \leq P_e \leq 1$. This leads to an *emission-current spike* around the stepping time t_1.

III. NUMERICAL RESULTS AND DISCUSSION

In our numerical calculation, we have chosen a QWIP sample 1 which contains GaAs layers as QWs and Al$_{0.3}$Ga$_{0.7}$As layers as barriers between adjacent wells. The well depth is $U_0=224$ meV, the well width is $L_W=50$ Å, the barrier thickness is $L_B=339$ Å, and the effective mass of electrons is $m^*=0.0665m_0$, with m_0 being the free-electron mass. The photon energy $\hbar\omega_{ph}$ is resonantly set to be the energy-level separation between the ground and first-excited states in the QWs with a homogeneous level broadening of 1 meV. The other parameters of sample 1 are listed in Table I. The parameter of another sample used in our measurement with time-dependent electric field is listed in Table II. The parameter of the sample used in the experiment by Hubbs et al. with a time-dependent optical flux can be found in Ref. 2. In this section, we will present both our numerical and experimental results for the QWIPs in the presence of a time-dependent electric field. After that, our calculated transient emission current will be displayed together with the experimental data from Ref. 2. Finally, we will show our calculated transient tunneling currents with a time-dependent device temperature.

TABLE II. GaAs/Al$_{0.3}$Ga$_{0.7}$As QWIP sample 2 used in our experiments in the presence of a time-dependent electric field with well width L_W, barrier thickness L_B, cross-sectional area S, and electron density n_{2D}.

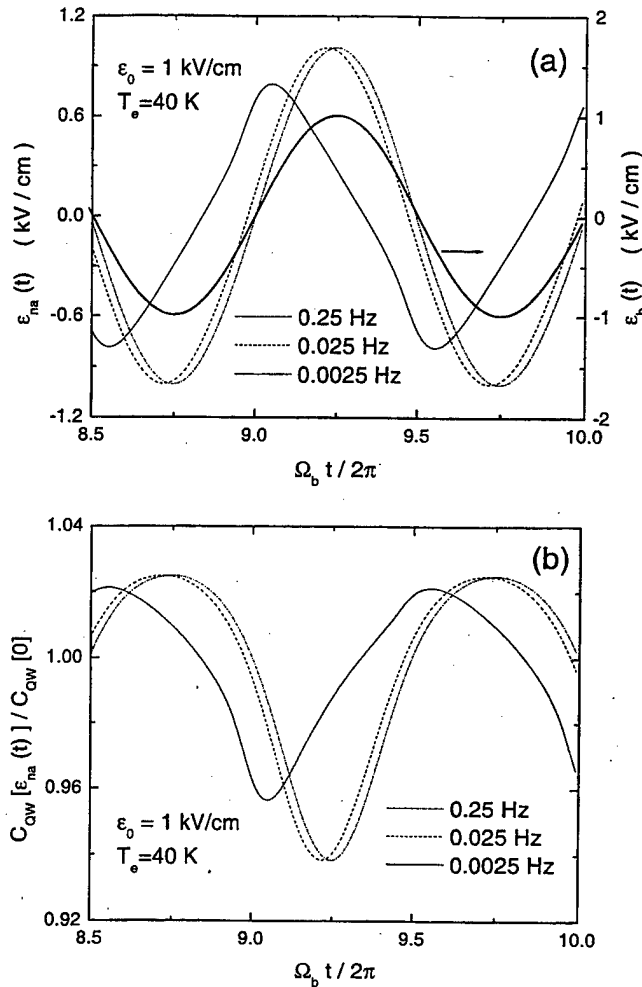| L_W (Å)	L_B (Å)	S (10^{-4} cm^{-2})	n_{2D} (10^{11} cm^{-2})
50	300	9	2.5

FIG. 1. Calculated $\mathcal{E}_{na}(t)$ [left axis in (a)] and $C_{QW}[\mathcal{E}_{na}(t)]/C_{QW}[0]$ [left axis in (b)] from sample 1 at $\mathcal{E}_0 = 1$ kV/cm and $T_e = 40$ K as a function of $\Omega_b t/2\pi$ for different frequencies $\Omega_b t/2\pi = 0.0025$ (thin solid curves), 0.025 (thin dashed curves), and 0.25 Hz (thin dash-dotted curves). $\mathcal{E}_b(t)$ [right axis in (a)] is also displayed by the thick solid curve for the comparison. Here, the curves are only shown for one time period for clarity.

A. Dynamical breakdown

For the time-dependent electric field, we choose a sinusoidal form

$$\mathcal{E}_b(t) = \mathcal{E}_0 \sin(\Omega_b t), \tag{10}$$

where $\mathcal{E}_0$ and Ω_b are the amplitude and oscillation frequency of $\mathcal{E}_b(t)$. In our numerical calculation, the tunneling time τ_t in Eq. (5) is evaluated using $e/I_t[\mathcal{E}_b(t), T_e]$, which depends on the time through $\mathcal{E}_b(t)$. In the following, we use sample 1 in our numerical calculation and sample 2 in our experimental measurement. In our experiment, an ac bias voltage is applied to sample 2 with its amplitude V_0 and oscillation frequency Ω_b.

The solution of Eq. (5) is presented in Fig. 1, where the nonadiabatic electric field $\mathcal{E}_{na}(t)$ [left axis in (a)] and the ratio of quantum-well capacitance $C_{QW}[\mathcal{E}_{na}(t)]/C_{QW}[0]$ [left axis in (b)] are shown as functions of $\Omega_b t/2\pi$ for different frequencies $\Omega_b t/2\pi = 0.0025$ (thin solid curves), 0.025 (thin dashed curves), and 0.25 Hz (thin dash-dotted curves). Here, we have chosen $\mathcal{E}_0 = 1$ kV/cm and $T_e = 40$ K in our calcula-

tion. When $\Omega_b/2\pi = 0.0025$ Hz, we find from (a) that $\mathcal{E}_{na}(t)$ changes periodically with time in a nonsinusoidal fashion due to the nonlinearity of Eq. (5) with respect to $\mathcal{E}_{na}(t)$. There is a $\pi/2$ phase shift between $\mathcal{E}_{na}(t)$ and $\mathcal{E}_b(t)$ (thick solid curve and right axis) because the former is linearly driven by $d\mathcal{E}_b(t)/dt$ instead of $\mathcal{E}_b(t)$ as seen from Eq. (5). As Ω_b increases, the phase shift disappears. The peak of $\mathcal{E}_{na}(t)$ first increases with Ω_b, but then saturates to a maximum value when $\Omega_b/2\pi > 0.025$ Hz, leading to the saturation of the tunneling-current peak. From Figs. 1(a) and 1(b) we find that $C_{QW}[\mathcal{E}_{na}(t)]$ and $\mathcal{E}_{na}(t)$ are out of phase with each other. This can be easily understood from the definition of $\mathcal{E}_{na}(t)$ in Eq. (4). The oscillations of $C_{QW}[\mathcal{E}_{na}(t)]/C_{QW}[0]$ with time reflect the switching between the charging and discharging status of the QWs. There is an asymmetry in the decay time constants due to different ratios of $C_{QW}[\mathcal{E}_{na}(t)]/C_{QW}[0]$ when the QWs are in the charged ($\mathcal{E}_{na}(t) < 0$) or discharged ($\mathcal{E}_{na}(t) > 0$) status.[4]

In Fig. 2 we present the calculated total current $I_t[\mathcal{E}_b(t) + \mathcal{E}_{na}(t), T_e] + \epsilon_0 \epsilon_r S d\mathcal{E}_b(t)/dt$ [left axis in (a)] and measured signal (proportional to the total current) [left axis in (b)] as a function of $\Omega_b t/2\pi$ for different frequencies $\Omega_b/2\pi$. In Fig. 2(a), we have picked $T_e = 40$ K and $\mathcal{E}_0 = 1$ kV/cm, and the thin solid, dashed, dotted, dash-dotted, and dash-dot-dotted curves correspond to $\Omega_b/2\pi = 0.02$, 0.2, 0.6, 1, and 2 Hz, respectively. In Fig. 2(b), $T_e = 40$ K and $V_0 = 9$ V are chosen, and the thin solid, dashed, dotted, dash-dotted, and dash-dot-dotted curves represent the results with $\Omega_b/2\pi = 50$, 20, 10, 5, and 2 kHz. $\mathcal{E}_b(t)$ and the ac bias voltage are also plotted for comparison using the thick solid curves in (a) and (b) (right axis). As can be seen from (a), the total current is almost in-phase with $\mathcal{E}_b(t)$ when $\Omega_b/2\pi = 0.02$ Hz. However, a $\pi/2$ phase shift is reached between the total current and $\mathcal{E}_b(t)$ when Ω_b becomes large. The strength of the shifted peak increases with Ω_b. This behavior can be explained as a result of the increased importance of the dielectric current compared to the tunneling current as Ω_b increases, as discussed in Sec. II B. This explanation is qualitatively supported by our experimental results shown in (b), where the peak position of the measured total current is gradually shifted from in-phase to out-of phase compared to the applied bias voltage and the peak strength is enhanced with the increase of Ω_b.

Figure 3 displays the extracted tunneling current and dielectric-current peaks [in (a)] from our calculation and total-current peaks [in (b)] from the measurement as a function of $\Omega_b/2\pi$ on a logarithmic scale. In Fig. 3(a) the thick solid, dashed, and dash-dotted curves correspond to the tunneling-current peaks at $T_e = 40$ K and $\mathcal{E}_0 = 10$ kV/cm, $T_e = 10$ K and $\mathcal{E}_0 = 10$ kV/cm, and $T_e = 40$ K and $\mathcal{E}_0 = 1$ kV/cm, respectively. The thin solid and dash-dotted curves represent the dielectric-current peaks with $\mathcal{E}_0 = 10$ kV/cm and $\mathcal{E}_0 = 1$ kV/cm. From Fig. 3(a) we find that the tunneling-current peak is relatively large when Ω_b is small, but the dielectric-current peak eventually dominates when Ω_b is large due to the saturation of the tunneling-current peak with Ω_b. The turning points Ω_b^* are indicated by the vertical arrows in (a) for each case, which depends on T_e and $\mathcal{E}_0$. When Ω_b goes beyond Ω_b^*, the photodetectors
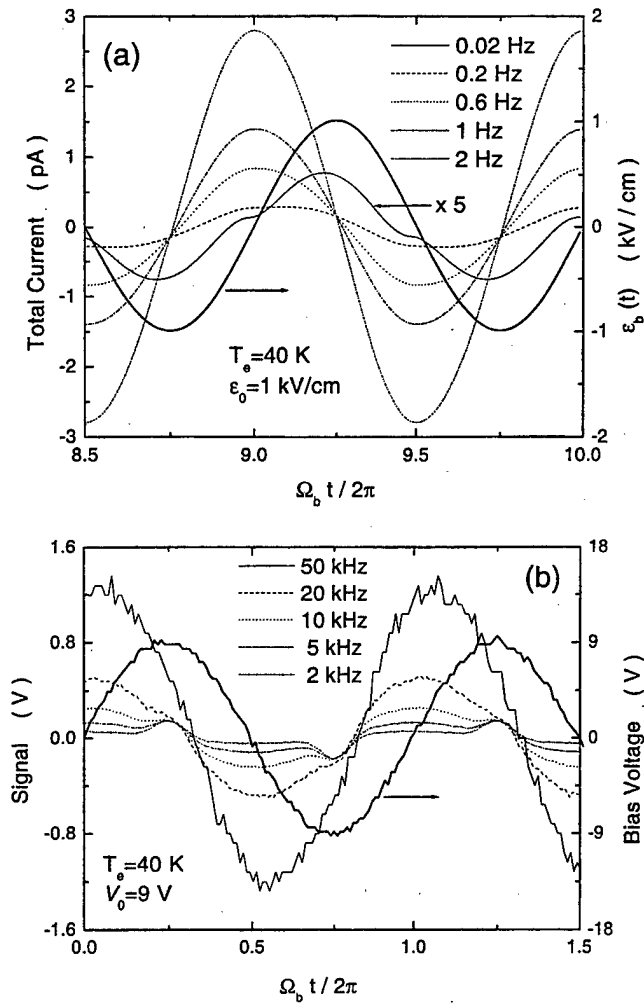
FIG. 2. Calculated total current (sum of the tunneling and dielectric currents) from sample 1 [left axis in (a)] and measured signal (proportional to the total current) from sample 2 [left axis in (b)] at $T_e = 40$ K as functions of $\Omega_b t/2\pi$ for different frequencies $\Omega_b/2\pi$. $\mathcal{E}_b(t)$ and ac bias voltage are also plotted for comparison using thick solid curves [right axis in (a) and (b)]. We have set in (a) $\mathcal{E}_0 = 1$ kV/cm, and the thin solid, dashed, dotted, dash-dotted, and dash-dot-dotted curves correspond to $\Omega_b/2\pi = 0.02$, 0.2, 0.6, 1, and 2 Hz. The label ×5 indicates the factor of amplification for the thin solid curve. In (b), we have set $V_0 = 9$ V, and the thin solid, dashed, dotted, dash-dotted, and dash-dot-dotted curves correspond to $\Omega_b/2\pi = 50$, 20, 10, 5, and 2 kHz. Here, the curves are only shown for one time period for clarity.

suffer from a *dynamical breakdown*. Ω_b^* can be estimated by $1/\mathcal{R}_t C_g$, where $C_g = \epsilon_0 \epsilon_r S/L_t$ with total length L_t of the QWIP and $\mathcal{R}_t$ is the sequential-tunneling resistance depending on T_e and $\mathcal{E}_0$. If T_e is high, Ω_b^* becomes large due to lower $\mathcal{R}_t$ (by comparing dashed and solid arrows). For the same reason, Ω_b^* increases with $\mathcal{E}_0$ (by comparing dash-dotted and solid arrows). This explanation is qualitatively confirmed by our experimental results shown in Fig. 3(b), where the solid and dashed curves represent the results at $T_e = 40$ and 10 K, and the symbols ($\square$, $\triangle$, $\bigstar$, and $\bullet$) correspond to the total-current peaks with $V_0 = 10$, 7.5, 5, and 3 V, respectively.

B. Emission-current spike

For the time-dependent incident optical flux $\Phi_{ph}(t)$, we will use a periodic or a step function for an optical chopper or an optical shutter, respectively. $\Phi_{ph}(t)$ is given by
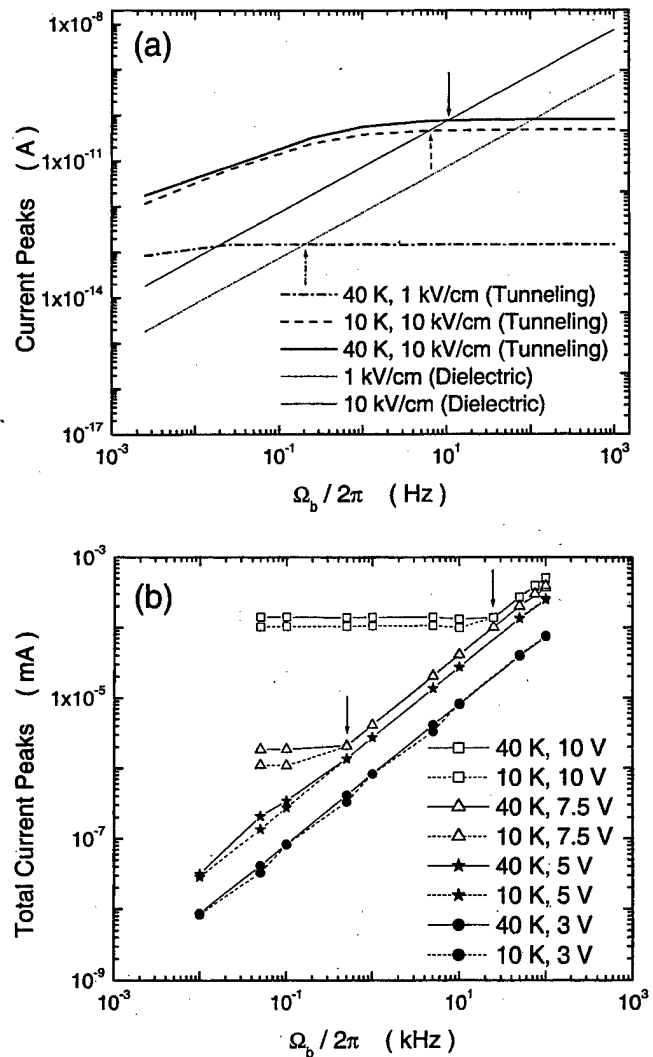
FIG. 3. Calculated logarithmic tunneling-current (thick curves) and dielectric-current (thin curves) peaks from sample 1 [in (a)] and measured logarithmic total-current peaks from sample 2 [in (b)] as functions of $\Omega_b t/2\pi$ in a logarithmic scale for different values of T_e and $\mathcal{E}_0$ in (a) or T_e and V_0 in (b). In (a), the thick solid, dashed, and dash-dotted curves represent the tunneling-current peaks with $T_e = 40$ K and $\mathcal{E}_0 = 10$ kV/cm, $T_e = 10$ K and $\mathcal{E}_0 = 10$ kV/cm, and $T_e = 40$ K and $\mathcal{E}_0 = 1$ kV/cm, respectively. The thin solid and dash-dotted curves correspond to the dielectric-current peaks with $\mathcal{E}_0 = 10$ and 1 kV/cm. The solid and dashed curves in (b) represent the results of measured total-current peaks at $T_e = 40$ and 10 K, respectively, with $V_0 = 10$ ($\square$), 7.5 ($\triangle$), 5 ($\bigstar$), and 3 V ($\bullet$). The vertical arrows in (a) and (b) indicate the turning points of Ω_b^*, and the dynamical breakdown occurs beyond those values.

$$\Phi_{ph}(t) = \begin{cases} \Phi_0 + \Delta\Phi P(t) & \text{for an optical chopper} \\ \Phi_0 + \Delta\Phi\, \theta(t) & \text{for an optical shutter} \end{cases}, \tag{11}$$

where $\Delta\Phi$ is the step height and Φ_0 is the background optical flux. Moreover, $\theta(t)$ is a step function which steps up at $t = 0$, and $P(t)$ is a unit periodic square-wave function given by

$$P(t) = \begin{cases} 0 & \text{if } mT_p \leqslant t < (m+1/2)T_p \\ 1 & \text{if } (m+1/2)T_p \leqslant t < (m+1)T_p \end{cases}. \tag{12}$$

In Eq. (12), $m = 0$, ± 1, ± 2,..., T_p is the time period, and $P(t)$ steps up at $t = (m+1/2)T_p$ and steps down at $t = (m$
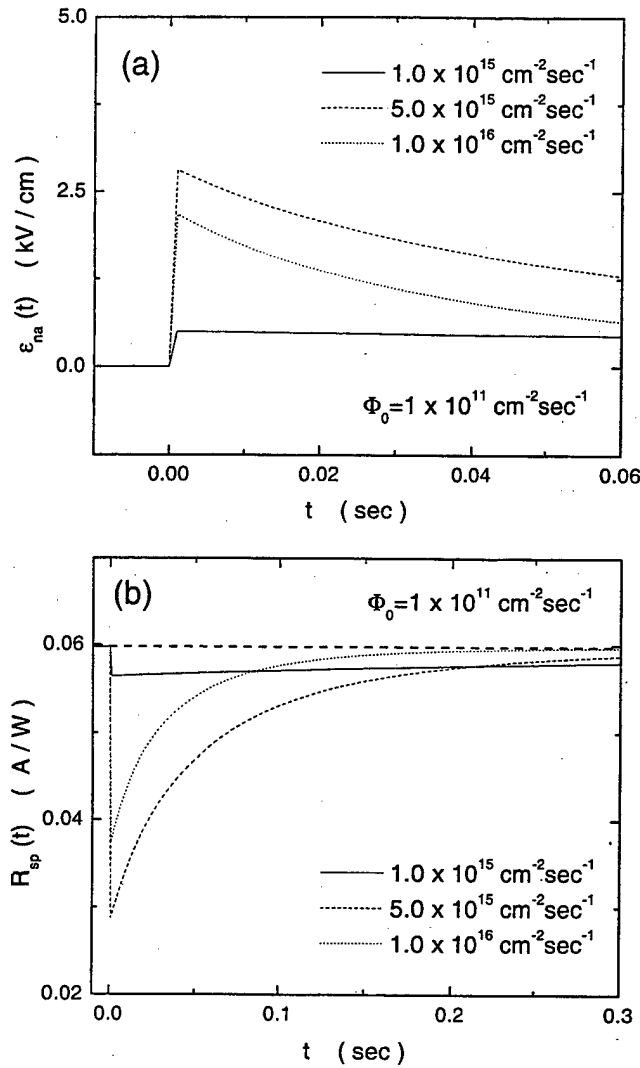
FIG. 4. Calculated $\mathcal{E}_{na}(t)$ [in (a)] and transient responsivity $R_{sp}(t)$ [in (b)] from sample 1 at $T_e = 40$ K, $\mathcal{E}_b = 2$ kV/cm, and $\Phi_0 = 1 \times 10^{11}$ cm^{-2} s^{-1} as functions of time for different step heights $\Delta\Phi = 1$ (thin solid curves), 5 (thin dashed curves), and 10×10^{15} cm^{-2} s^{-1} (thin dotted curves) in the presence of an optical shutter opening at $t = 0$. The static responsivity is also shown by a thick dashed line in (b) for comparison.

$+1)T_p$. In our numerical calculation, the excited-state lifetime τ_i in Eq. (8) is taken to be 1 ps, the electron temperature is $T_e = 40$ K, and a dc electric field $\mathcal{E}_b = 2$ kV/cm is applied to the sample in the z direction. In the following, we still use sample 1 in our numerical calculation. Some experimental results from Ref. 2 are also shown for a qualitative comparison with our calculated results.

Figure 4 displays the solution of Eq. (8) in the presence of an optical shutter which opens at $t = 0$, where the nonadiabatic electric field $\mathcal{E}_{na}(t)$ [in (a)] and the transient responsivity $R_{sp}(t)$ [in (b)] are shown as a function of time for different step heights $\Delta\Phi = 1 \times 10^{15}$ (thin solid curves), 5 $\times 10^{15}$ (thin dashed curves), and 10×10^{15} cm^{-2} s^{-1} (thin dotted curves). Here, we have chosen $\mathcal{E}_b = 10$ kV/cm, $T_e = 40$ K, and $\Phi_0 = 1 \times 10^{11}$ cm^{-2} s^{-1} in our calculation. The static responsivity is also shown by the thick dashed line in (b) for comparison. From (a) we know that $\mathcal{E}_{na}(t) > 0$ after the shutter is opened, indicating a discharged status for the

QWs during a series of intermediate transient states. $\mathcal{E}_{na}(t)$ has an initial rise just after the shutter is opened. Once $d\Phi_{ph}(t)/dt = 0$ is reached, $\mathcal{E}_{na}(t)$ goes through a decay down to zero. Consequently, the electrons in the QWs are stabilized by entering into a final steady state with a higher emission current but the same tunneling current. The initial rise of $\mathcal{E}_{na}(t)$ becomes steeper and steeper and the final decay becomes faster and faster as $\Delta\Phi$ is increased. From (b) we find that transient responsivity $R_{sp}(t)$ is always smaller than its static counterpart because of the loss of electrons in the discharged QWs. The initial drop of $R_{sp}(t)$ due to the steep rise of $\mathcal{E}_{na}(t)$ becomes deeper and deeper, which is followed by a final decay to its static value with an enhanced rate as $\Delta\Phi$ increases. In the adiabatic case, the photoemission current is proportional to $\Phi_{ph}(t)$, which gives rise to the static responsivity.[5,6] The transient responsivity depends on the time through $\mathcal{E}_{na}(t)$ which depends on $\Phi_{ph}(t)$ in the nonadiabatic case, implying a nonlinear relation between the photoemission current and $\Phi_{ph}(t)$.

In Fig. 5 we present the calculated total ac current $I_e[\mathcal{E}_b + \mathcal{E}_{na}(t), \Phi_{ph}(t)] + \Delta I_t(t)$ with $\Delta I_t(t) = I_t[\mathcal{E}_b + \mathcal{E}_{na}(t), T_e] - I_t[\mathcal{E}_b, T_e]$ [in (a)] and the measured total ac signal (proportional to the total ac current) [in (b)] for an optical shutter as a function of time. In (a), we set $\mathcal{E}_b = 2$ kV/cm, $T_e = 40$ K, and $\Phi_0 = 1 \times 10^{11}$ cm^{-2} s^{-1} in our calculation and the solid, dashed, dotted, dash-dotted, and dash-dot-dotted curves correspond to the step heights $\Delta\Phi = 1, 5, 10, 20$, and 40×10^{15} cm^{-2} s^{-1}, respectively. In (b), a dc bias voltage $V_b = 1$ V is applied and $T_e = 43$ K and $\Phi_0 = 1.1 \times 10^{13}$ cm^{-2} s^{-1} are chosen. The 11 curves from the bottom to the top represent the results with $\Delta\Phi = 4.5, 6.1, 7.0, 8.07, 8.5, 12.9, 15.9, 18.9, 21.9$, and 25.9×10^{13} cm^{-2} s^{-1}, respectively. From (a), we find that the step height of the total ac current increases with $\Delta\Phi$ after the shutter is opened. The rise and decay time becomes shorter as $\Delta\Phi$ increases. Moreover, an *emission-current spike* occurs when $\Delta\Phi = 4 \times 10^{16}$ cm^{-2} s^{-1}. The decreasing rise and decay time results from the reduced $C_{QW}[\mathcal{E}_{na}(t)]$ due to the enhancement of a positive $\mathcal{E}_{na}(t)$ with $\Delta\Phi$ as shown in Fig. 4(a). The emission-current spike is a result of the competition between the exponential enhancement of the escape probability with respect to $\mathcal{E}_{na}(t)$ and the linear reduction of electron density with respect to $\mathcal{E}_{na}(t)$ due to the loss of electrons in each QW, as explained in Sec. II C. This explanation is qualitatively supported by the experimental data from Ref. 2 in Fig. 5(b), where both the occurrence of the emission-current spike and the shortening of the rise and decay time are observed with increasing $\Delta\Phi$.

Calculated total ac currents $I_e[\mathcal{E}_b + \mathcal{E}_{na}(t), \Phi_{ph}(t)] + \Delta I_t(t)$ (thick solid curves) with an optical chopper are shown in Fig. 6 as a function of time for different time periods $T_p = 0.1$ [in (a)] and 0.5 s [in (b)]. Here, we set $\mathcal{E}_b = 2$ kV/cm, $T_e = 40$ K, $\Phi_0 = 1 \times 10^{11}$ cm^{-2} s^{-1}, and $\Delta\Phi = 4.3 \times 10^{16}$ cm^{-2} s^{-1} in our calculation. The adiabatic emission currents $I_e[\mathcal{E}_b, \Phi_{ph}(t)]$ are also shown in both Figs. 6(a) and 6(b) by the thin dotted curves for comparison. From (a) and (b), we find that the rising time is always relatively shorter than the descending time within the decaying region with $\Phi_{ph}(t) = \Phi_0$. The rising and descending processes are
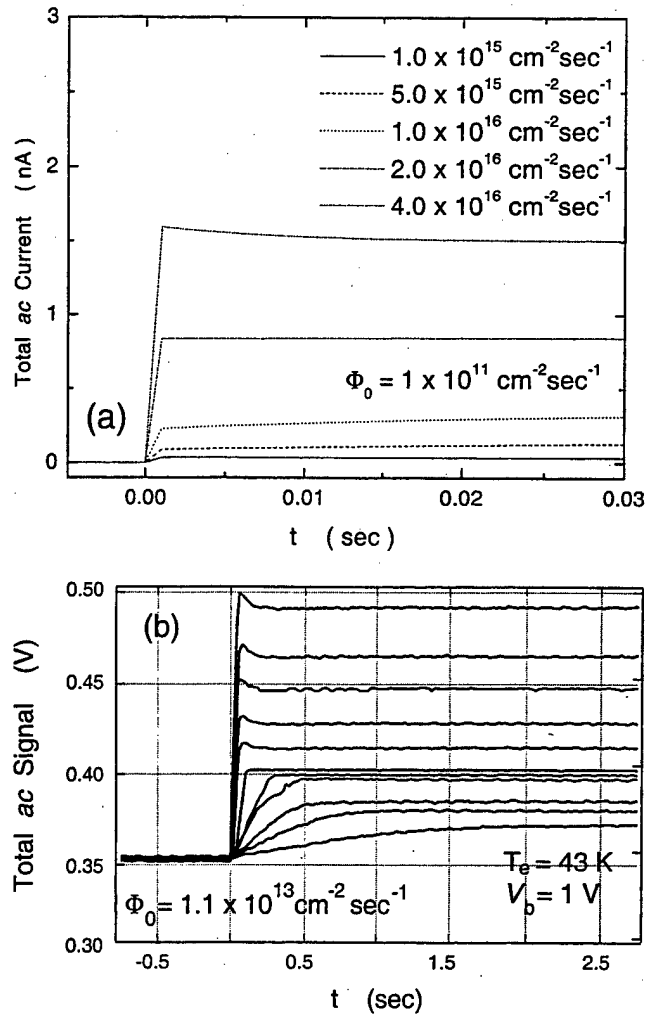
FIG. 5. Calculated total ac current $I_e[\mathcal{E}_b+\mathcal{E}_{na}(t), \Phi_{ph}(t)]+\Delta I_t(t)$ from sample 1 [in (a)] with transient part of tunneling current $\Delta I_t(t)=I_t[\mathcal{E}_b +\mathcal{E}_{na}(t),T_e]-I_t[\mathcal{E}_b,T_e]$ and the measured total ac signal (proportional to the total ac current) [in (b)] from Ref. 2 as functions of time for an optical shutter opening at $t=0$. We set in (a) $\mathcal{E}_b=2$ kV/cm, $T_e=40$ K, and $\Phi_0=1 \times 10^{11}$ cm^{-2} s^{-1} in our calculation, and the solid, dashed, dotted, dash-dotted, and dash-dot-dotted curves correspond to $\Delta\Phi=1, 5, 10, 20,$ and 40 $\times 10^{15}$ cm^{-2} s^{-1}, respectively. In (b), a dc bias voltage $\mathcal{V}_b=1$ V is applied to the sample, and $T_e=43$ K and $\Phi_0=1.1 \times 10^{13}$ cm^{-2} s^{-1} are chosen. The 11 curves from the bottom to the top represent the results with $\Delta\Phi=4.5, 6.1, 7.0, 8.07, 8.5, 12.9, 15.9, 18.9, 21.9,$ and 25.9×10^{13} cm^{-2} s^{-1}, respectively.

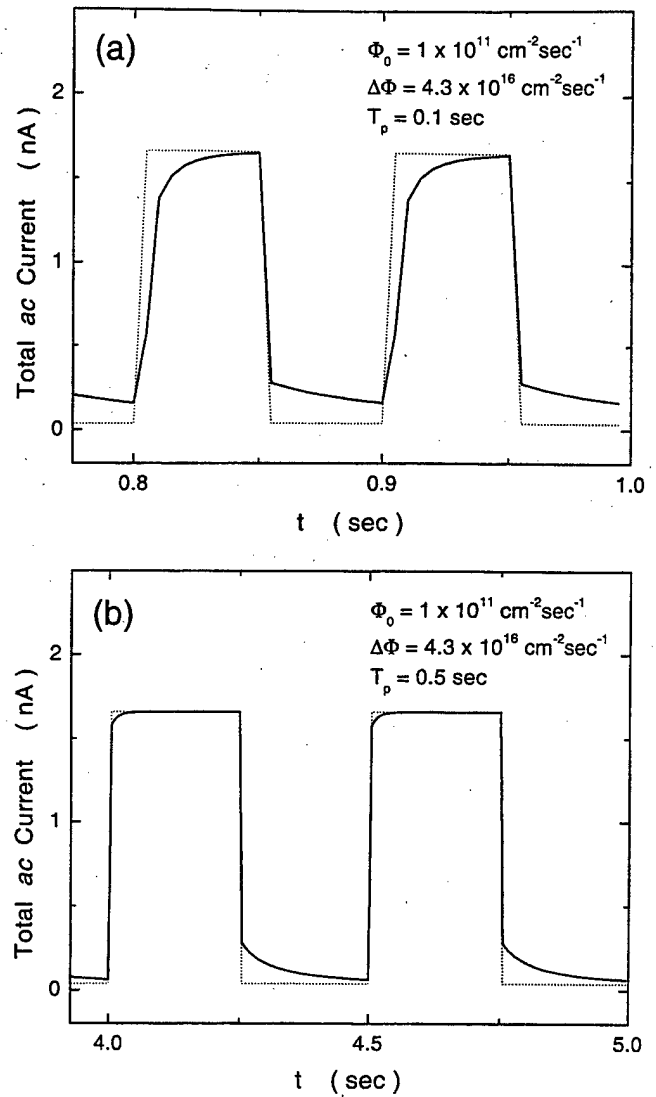FIG. 6. Calculated total ac current $I_e[\mathcal{E}_b+\mathcal{E}_{na}(t),\Phi_{ph}(t)]+\Delta I_t(t)$ (thick solid curves) with $\Delta I_t(t)=I_t[\mathcal{E}_b+\mathcal{E}_{na}(t),T_e]-I_t[\mathcal{E}_b,T_e]$ from sample 1 at $T_e=40$ K, $\mathcal{E}_b=2$ kV/cm, $\Phi_0=1\times10^{11}$ cm^{-2} s^{-1}, and $\Delta\Phi=4.3 \times 10^{16}$ cm^{-2} s^{-1} as a function of time for an optical chopper with $T_p=0.1$ [in (a)] and 0.5 s [in (b)]. For comparison, the adiabatic emission currents $I_e[\mathcal{E}_b,\Phi_{ph}(t)]$ are also shown by the thin dotted curves in both (a) and (b). Here, the curves are only shown for two time periods for clarity.

slower in (a) with respect to (b). A larger residual ac current is found in (a) at the end of a decaying process. These features predicted by our theory agree well with the measured total ac signals from Ref. 2 presented in Fig. 7 for $T_p=5$ [in (a)] and 20 s [in (b)], where $\mathcal{V}_b=1$ V, $T_e=43$ K, $\Phi_0=1.1 \times 10^{13}$ cm^{-2} s^{-1}, and $\Delta\Phi=6.1\times10^{13}$ cm^{-2} s^{-1} are chosen in the experiment.

C. Thermal hysteresis loop

For the time-dependent device temperature, we pick a broadened staircase form

$$T_e(t)=T_0+\Delta T\sum_{j=1}^{N_s}\left\{\frac{1}{2}+\frac{1}{\pi}\tan^{-1}\left[\frac{t-(j-1)\Delta t-t_1}{\Gamma}\right]\right\},$$

(13)

where j is the index of the step, N_s is the total number of steps, t_1 is the first stepping time, T_0 is the initial temperature, and Δt, ΔT, and Γ are, respectively, the delay time, step height, and step broadening. In our numerical calculation, the energy-relaxation time τ_r in Eq. (3) is taken to be 1 ps. The temperature evolution with time can be realized by turning on/off the heater at the stepping time for stepping up/down, respectively. In the following, we choose sample 1 for our numerical calculation.

Figure 8 shows the calculated nonadiabatic (left axis and solid curves) and adiabatic (left axis and dashed curves) tunneling currents with $\mathcal{E}_b=5$ kV/cm, $N_s=1$, $t_1=500$ s and $\Gamma=30$ s as a function of time for different initial temperatures T_0 [in (a)] and for positive/negative ΔT [in (b)]. In (a), $\Delta T=5$ K is chosen, and the thick and thin curves represent the results with $T_0=30$ and 10 K. The time-dependent device
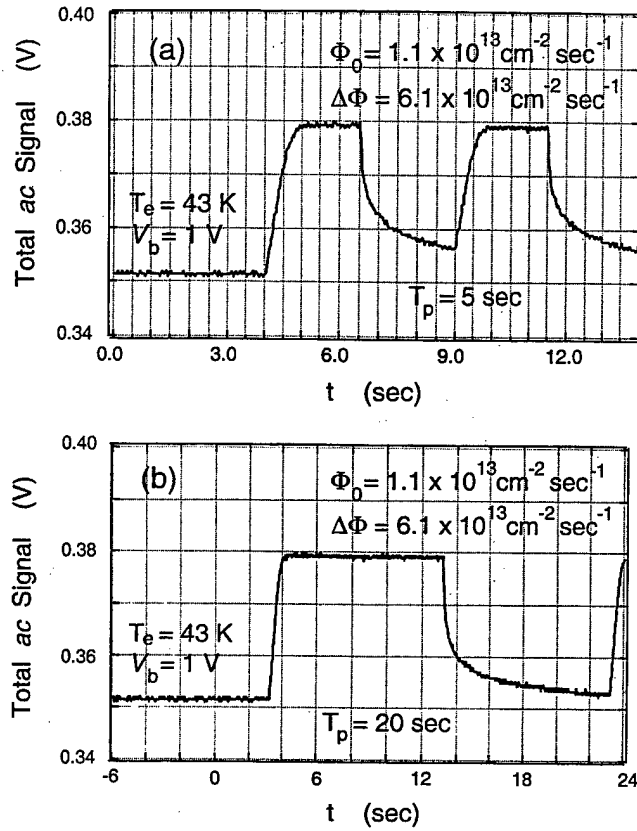
.FIG. 7. Measured total ac signals (proportional to the total ac currents) from Ref. 2 as functions of time for an optical chopper with $T_p = 5$ [in (a)] and 20 s [in (b)]. In the experiment, a dc bias voltage $V_b = 1$ V is applied to the sample, and $T_e = 43$ K, $\Phi_0 = 1.1 \times 10^{13}$ cm^{-2} s^{-1}, and $\Delta\Phi = 6.1 \times 10^{13}$ cm^{-2} s^{-1} are chosen. Here, the curves are only shown for one time period for clarity.
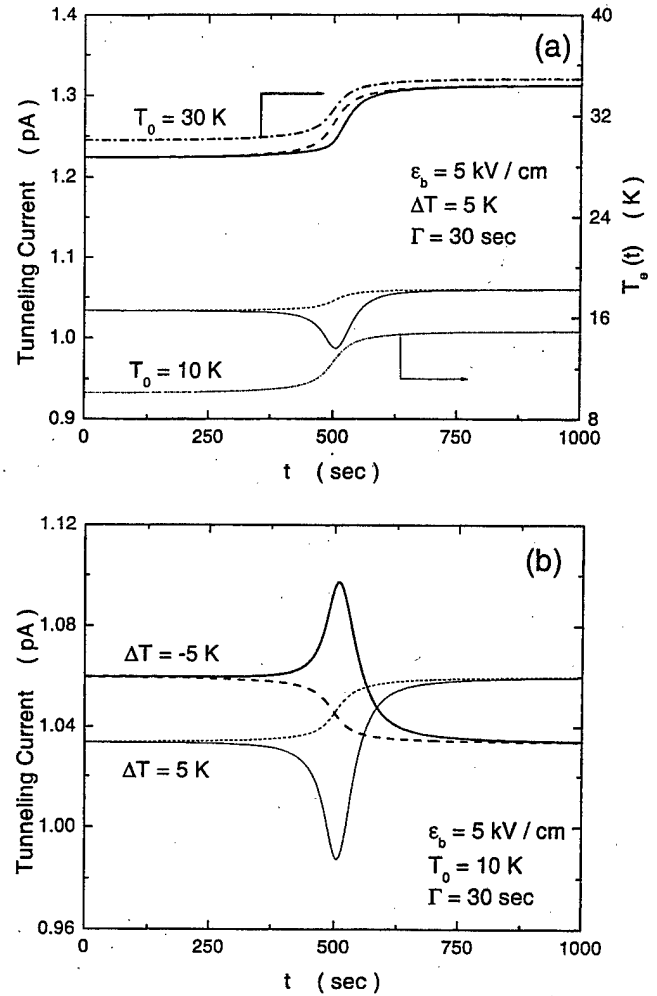

FIG. 8. Calculated nonadiabatic tunneling currents $I_t[\mathcal{E}_b + \mathcal{E}_{na}(t), T_e(t)]$ (left axis and solid curves) and adiabatic tunneling currents $I_t[\mathcal{E}_b, T_e(t)]$ (left axis and dashed curves) from sample 1 at $\mathcal{E}_b = 5$ kV/cm as functions of time for different initial temperatures T_0 [in (a)] and positive/negative step heights ΔT [in (b)], where $N_s = 1$, $\Gamma = 30$ s, and $t_1 = 500$ s. We have set in (a) $\Delta T = 5$ K, and the thick and thin curves correspond to $T_0 = 30$ and 10 K. For comparison, $T_e(t)$ as a function of time is also shown by the dash-dotted curves (right axis). In (b), $T_0 = 10$ K is chosen, and the thick and thin curves represent the results with $\Delta T = -5$ and 5 K.

temperature $T_e(t)$ is also displayed by the dash-dotted curves (right axis). In (b), $T_0 = 10$ K is taken, and the thick and thin curves correspond to $\Delta T = -5$ and 5 K. From Fig. 8(a), we find that the nonadiabatic current (solid curves) is always smaller than the adiabatic one (dashed curves) when the temperature steps up. The amplitude of the reduction of $I_t[\mathcal{E}_b + \mathcal{E}_{na}(t), T_e(t)]$ with respect to $I_t[\mathcal{E}_b, T_e(t)]$ increases with decreased T_0, and gradually develops into a dip when T_0 is down to 10 K. The reason for this feature is that charge accumulation ($\mathcal{E}_{na}(t) < 0$) in the QWs blocks the sequential tunneling of electrons into the QWs, as explained in Sec. II A. From Fig. 8(b), we see $I_t[\mathcal{E}_b + \mathcal{E}_{na}(t), T_e(t)]$ $< I_t[\mathcal{E}_b, T_e(t)]$ (thin curves) when $T_e(t)$ steps up, as discussed in (a), but $I_t[\mathcal{E}_b + \mathcal{E}_{na}(t), T_e(t)] > I_t[\mathcal{E}_b, T_e(t)]$ (thick curves) when $T_e(t)$ steps down. This implies a counterclockwise *thermal hysteresis loop* in the tunneling current as a function of $T_e(t)$, which will be further addressed below.

Figure 9 presents the solutions $\mathcal{E}_{na}(t)$ of Eq. (3) [left axis and thick curves in (a)] and the calculated nonadiabatic tunneling currents $I_t[\mathcal{E}_b + \mathcal{E}_{na}(t), T_e(t)]$ [thick curves in (b)] as functions of time with $\mathcal{E}_b = 1$ kV/cm, $N_s = 8$, $t_1 = 200$ s, $\Gamma = 30$ s, and $\Delta t = 100$ s for $\Delta T = -5$ K (solid curves) and 5 K (dashed curves). For convenience, the device temperature profiles $T_e(t)$ [right axis in (a)] and the calculated adiabatic tunneling currents $I_t[\mathcal{E}_b, T_e(t)]$ [in (b)] as functions of time are also displayed for $\Delta T = -5$ K (thin solid curves) and 5 K

(thin dashed curves). From Fig. 9(a), we find that $\mathcal{E}_{na}(t)$ (thick solid curve) remains positive and exhibits an oscillating feature when the device temperature is swept down from 50 to 30 K, indicating a modulated discharging status for the QWs. On the other hand, when the device temperature is swept up from 30 to 50 K, $\mathcal{E}_{na}(t)$ (the thick dashed curve) is found to be negative and oscillating with time, resulting from a modulated charging status for the QWs. From Fig. 9(b), we see $I_t[\mathcal{E}_b + \mathcal{E}_{na}(t), T_e(t)]$ (thick solid curve) shows a strong oscillation and an enhancement compared to $I_t[\mathcal{E}_b, T_e(t)]$ (thin solid curve) when the temperature is swept down. The reason for this is that the loss of electrons in the QWs in a modulated discharging status promotes the sequential tunneling of electrons into the QWs through the space-charge-field effect.[4] Based on the same concept of a space-charge-field, we can easily understand that $I_t[\mathcal{E}_b + \mathcal{E}_{na}(t), T_e(t)]$ (thick dashed curve) will have a partial suppression compared to $I_t[\mathcal{E}_b, T_e(t)]$ (thin dashed curve) as the temperature is swept
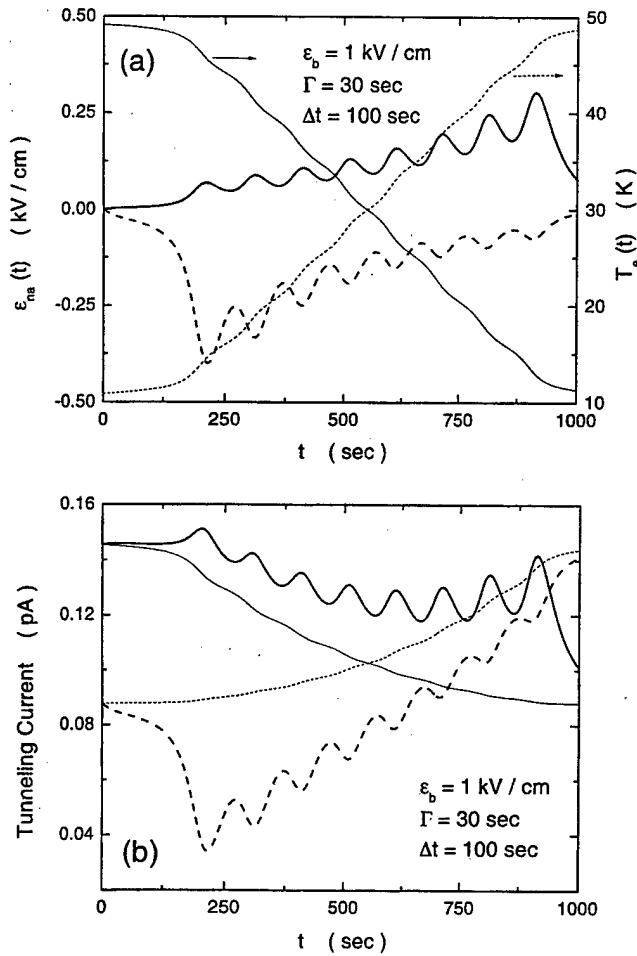
FIG. 9. Calculated nonadiabatic electric field $\mathcal{E}_{na}(t)$ (left axis and thick curves) and profile of $T_e(t)$ (right axis and thin curves) in (a) from sample 1, as well as the calculated tunneling currents $I_t[\mathcal{E}_b+\mathcal{E}_{na}(t),T_e(t)]$ (thick curves) and $I_t[\mathcal{E}_b,T_e(t)]$ (thin curves) in (b), at $\mathcal{E}_b=1$ kV/cm as functions of time for positive/negative step heights ΔT, where $N_s=8$, $t_1=200$ s, $\Gamma=30$ s, and $\Delta t=100$ s. In (a), $\Delta T=-5$ and 5 K correspond to solid and dashed curves. We set in (b) $\Delta T=-5$ and 5 K represented by the solid and dashed curves, respectively.

up due to a blocking of the sequential tunneling of electrons by the accumulation of electrons in the QWs.

In Fig. 10 we show the calculated nonadiabatic (thick curves) and adiabatic (thin dotted curves) tunneling currents using $N_s=8$, $t_1=200$ s, $\Gamma=30$ s, and $\Delta t=100$ s as a function of $T_e(t)$, respectively, for different dc electric fields $\mathcal{E}_b$ $=1$ kV/cm [in (a)] and 10 kV/cm [in (b)] with $\Delta T=-5$ K (thick solid curves) and 5 K (thick dashed curves). From Fig. 10(a), we find that the nonadiabatic tunneling current $I_t[\mathcal{E}_b +\mathcal{E}_{na}(t),T_e(t)]$ (thick dashed curve) goes up with increased $T_e(t)$ accompanied by a partial suppression in comparison with $I_t[\mathcal{E}_b,T_e(t)]$ (thin dotted curve), as explained in Fig. 9. On the other hand, $I_t[\mathcal{E}_b+\mathcal{E}_{na}(t),T_e(t)]$ (thick solid curve) goes down with decreased $T_e(t)$ accompanied by an enhancement in comparison with $I_t[\mathcal{E}_b,T_e(t)]$. As a result, a counterclockwise loop of tunneling current due to the thermal hysteresis loop is formed as the device temperature is first swept up and then swept down. The deviation of the nonadiabatic tunneling current from the adiabatic one becomes smaller as the device temperature is increased. This
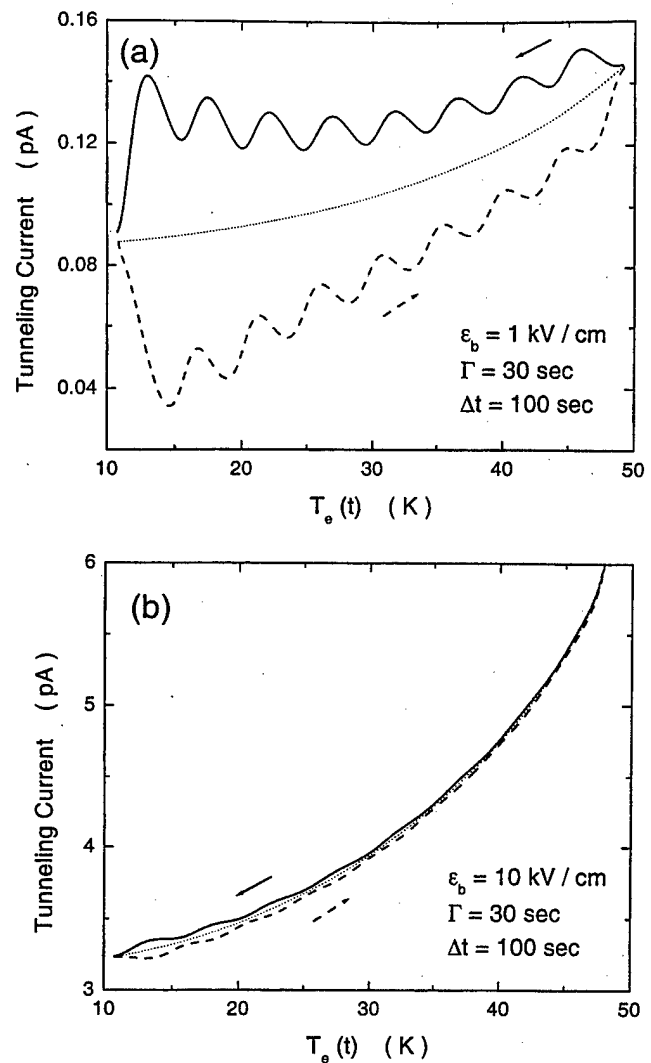

FIG. 10. Calculated tunneling currents $I_t[\mathcal{E}_b+\mathcal{E}_{na}(t),T_e(t)]$ (thick curves) and $I_t[\mathcal{E}_b,T_e(t)]$ (thin dotted curves) from sample 1 at $\mathcal{E}_b=1$ kV/cm as functions of devive temperature $T_e(t)$ for different dc electric fields $\mathcal{E}_b=1$ and 10 kV/cm. In both (a) and (b), the results with positive and negative step heights $\Delta T=\pm 5$ K are represented by the thick dashed and solid curves, where $N_s=8$, $t_1=200$ s, $\Gamma=30$ s, and $\Delta t=100$ s. Here, the solid (down) and dashed (up) arrows indicate the directions that the device temperature is swept down or up.

thermal hysteresis loop in the tunneling current was reported before by Choi et al.[3] However, a different explanation, which is attributed to the effects of unintentional dopants in the QWIP barriers, was provided for this observed phenomenon compared with the one given here. The thermal hysteresis loop can be effectively suppressed by applying a larger dc electric field, as shown in Fig. 10(b) because the tunneling resistance will be reduced by increasing either the temperature or the bias.[3]

IV. CONCLUSIONS AND REMARKS

In conclusion, a nonadiabatic sequential-tunneling model has been developed and used to explore the common origin of the transient behaviors of electrons in QWIPs in the presence of time-dependent external sources such as device temperature, electric field, and incident optical flux. The nona-

diabatic effect of a time-dependent source includes the charge-density fluctuation in the QWs induced by a nonadiabatic current surge. The results from our numerical calculations have been qualitatively compared with our experimental data and those from the experiment in Ref. 2 by Hubbs et al. The experimental observations have been reproduced numerically and explained physically.

For a time-dependent device temperature, a counterclockwise hysteresis loop for the tunneling current as a function of swept temperature has been predicted and attributed to the blockade or promotion of sequential tunneling of electrons into the QWs due to a modulated space-charge field when the device temperature is swept up and then down. When a time-dependent electric field is applied to the system, the peak of the tunneling current was found to saturate when the oscillation frequency of the ac electric field was large enough. The dynamical breakdown of photodetectors has been predicted by including a dielectric current, which is proportional to the oscillation frequency of an ac electric field and whose peak becomes larger than the value of the saturated tunneling-current peak in the high-frequency domain. If an incident optical flux becomes time dependent, an emission-current spike was predicted as a result of the dominant enhancement of the escape probability of electrons in QWs over the loss of electron density when the applied dc electric field is small.

The report of a clockwise hysteresis loop for the emission current as a function of swept temperature by Choi et al. in Ref. 3 can also be explained by our model. From our present study, we find that the QWs remain either in a charged ($\mathcal{E}_{na}(t) < 0$) or a discharged ($\mathcal{E}_{na}(t) > 0$) transient status when the device temperature is swept up or down, respectively [see Fig. 9(a)]. From our previous studies,[4] we know that the nonadiabatic tunneling current $I_t[\mathcal{E}_b + \mathcal{E}_{na}(t), T_e(t)]$ increases with $\mathcal{E}_{na}(t)$. However, the nonadiabatic emission current $I_e[\mathcal{E}_b + \mathcal{E}_{na}(t), \Phi_{ph}(t)]$ decreases as $\mathcal{E}_{na}(t)$ increases.[5] Consequently, from the counterclockwise hysteresis loop of the tunneling current we would predict a clockwise loop for the emission current[3] when the device temperature is swept up and then down.

Finally, we would like to mention that we have incorporated the charge-density fluctuation into our model simply by

deriving a dynamical nonadiabatic electric field which is spatially uniform. This nonadiabatic field results from the space charge in the system, and should be position dependent and obtained from Poisson's equation in general. In this way, the doping profile inside the QWIPs, in addition to electron density, will have an effect on the magnitude of the nonadiabatic field. Also, it has become well known that the imbalance between the injection current through the emitter and the emission current from the QWs can cause a nonuniform distribution of the applied bias voltage across the QWIP structure.[11,12] However, this effect can be minimized when the number of QWs in the QWIP is large. The present features predicted by our nonadiabatic model in this article remain valid after including the nonuniform distribution of the bias voltage inside the sample, although some quantitative difference is expected.

ACKNOWLEDGMENTS

[1] A. Singh and D. A. Cardimona, Opt. Eng. (Bellingham) **38**, 1424 (1999).

[2] J. E. Hubbs, D. C. Arrington, M. E. Grammer, and G. A. Dole, Opt. Eng. (Bellingham) **39**, 2660 (2000).

[3] K. K. Choi, S. W. Kennerly, J. Yao, and D. C. Tsui, Infrared Phys. Technol. **42**, 221 (2001).

[4] D. H. Huang, A. Singh, and D. A. Cardimona, J. Appl. Phys. **87**, 2427 (2000).

[5] D. H. Huang, A. Singh, D. A. Cardimona, and C. Morath, J. Appl. Phys. **89**, 4429 (2001).

[6] B. F. Levine, J. Appl. Phys. **74**, R1 (1993).

[7] D. H. Huang, D. A. Cardimona, and A. Singh, Phys. Lett. A **243**, 335 (1998).

[8] G. Burmeister and K. Maschke, Phys. Rev. B **57**, 13050 (1998).

[9] M. Lindberg and S. W. Koch, Phys. Rev. B **38**, 3342 (1988).

[10] H. C. Liu, Appl. Phys. Lett. **60**, 1507 (1992).

[11] L. Thibaudeau, P. Bois, and J. Y. Duboz, J. Appl. Phys. **79**, 446 (1996).

[12] M. Ershov, H. C. Liu, M. Buchanan, Z. R. Wasilewski, and V. Ryzhii, Appl. Phys. Lett. **70**, 414 (1997).

[13] J. Oiknine-Schlesinger, M. Gerling, D. Gershoni, E. Ehrenfreund, and D. Ritter, Phys. Rev. B **61**, 10972 (2000).

[14] D. H. Huang and M. O. Manasreh, J. Appl. Phys. **80**, 6045 (1996).

[15] J. D. Jackson, Classical Electrodynamics, 2nd ed. (Wiley, New York, 1975), Chap. 6.